C h a p t e r   1

INTRODUCTION

1.1 Background

Photochemical transformations present utility in synthetic chemistry as such mechanisms are highly specific and thus can provide control over the generated products.[1] Photons are extremely versatile synthetic reagents. Defining the photon wavelength determines what reactions will be promoted and defining the intensity determines the rate, and over time, the extent, of those reactions. Spatial confinement of photo-driven chemical reactions using structured illumination is the basis for several mesoscale pattern design and structure growth techniques. Photolithography, a technique used extensively to generate patterned materials and specifically in the semiconductor industry and in the production of integrated circuits, typically utilizes an optical mask to effect an illumination field with spatially-varying intensity to selectively polymerize or decompose a layer of organic photoresist applied to heterogenous substrate defined patterns.[2-5] A secondary step, e.g. via physical vapor deposition or dry etching, is then typically utilized to realize the pattern defined by the mask in the target material. Direct-write techniques can combine patterning and material addition or subtraction into a single processing step.[6-9] Such direct-writing may be accomplished by utilizing scanning laser illumination to locally drive decomposition of precursor gas promoting deposition or effect material ablation. In the same manner, pattern generation may be achieved via light-directed electrochemical processing of semiconductor substrates. The absorption of supra-bandgap photons in photoactive semiconductor substrates immersed in a metal-ion solution can provide the driving force for deposition of

the metal. This effect has been used to generate arbitrarily patterned deposits on the surface by utilization of a photomask or scanning laser illumination.[10-14] In such processes, localized illumination results in the spatially confined generation of mobile charge carriers which are transported toward the solid/solution interface and drive localized electrochemical deposition.

In general, photomask methods, as well as direct-write methods based on scanning laser illumination, rely on localizing light incidence and thus material addition/subtraction by manipulating the incidence of the light rather than capitalizing on inherent light-interaction anisotropies in the evolving structures during growth.[6-9] Approaches based on the latter phenomenon may better realize the potential power of photo-mediated synthesis by capitalizing on additional characteristics of the input light field beyond the spatial intensity profile, e.g. the wavelength, polarization, and phase. Such methods may simultaneously provide for superior accommodation of the generation of subwavelength scale features, exceeding the conventional diffraction limit, and relax the requirement for spatially structured illumination.[15,16] Linearly polarized light can effect photopolymerization and/or photoalignment in liquid crystal systems, generating highly anisotropic structures oriented along or perpendicular to the electric field vector.[17-20] Photoelectrochemical metal deposition on Si micro- and nanowire arrays can effect a wavelength-dependent spatial decoration profile.[21,22] The photoinduced mass transport of photoisomerizable polymers in the immediate vicinity of Au or Ag nanoparticles can generate patterns in the subwavelength regime with anisotropy dictated by the light polarization.[23-26] A well-studied example of light-mediated synthesis that capitalizes on asymmetrical light-matter interactions is the plasmon-mediated generation of Ag nanoparticles wherein illumination in the presence of Ag seeds and a reducing agent promotes growth of structures with surface plasmon resonance wavelengths similar to the illumination wavelength.[27,28] This method can generate

prisms, plates, rods, and cubes as well as other structures with high monodispersity, and provide size tuneability via control of the illumination wavelength.[15] Plasmon-mediated growth of surface-affixed, triangular Ag nanoparticles during illumination with linearly polarized light results in spontaneous anisotropic orientation as well as a consistent size.[29] This synthetic process is governed by the anisotropies in the light-material interactions resulting from sensitivity to both the wavelength and polarization of the illumination, and thus provides for the maskless generation of uniform, oriented nanostructures.[15]

Figure 1.1. Phototropic growth of palm trees. In the northern hemisphere, growth towards the time-averaged solar azimuth results in a southern tilt.

Sunflowers display diurnal motion wherein leaf orientation follows the solar azimuth to optimize insolation interception.[30] Such motion in response to illumination is known as heliotropism and is exhibited by many photosynthetic plants, including cotton and bean, and also in the movement of several other organisms including flies and small crustaceans.[31-35] Significant effort has been directed towards the generation of biomimetic photoactuators that exhibit heliotropic response for a variety of purposes, including solar tracking for energy applications, remote triggering of chemical reactions, and construction of soft robots.[36-39]

Photoresponsive behavior is also demonstrated by palm trees which exhibit growth towards the time-averaged position of the sun to maximize solar-harvesting, resulting in a southern tilt in the northern hemisphere as the tree morphology responds adaptively to the incident illumination; Figure 1.1 presents an image of this growth behavior for palm trees in Pasadena, California.[40] Growth involving physical extension and material addition in a directional fashion in response to illumination is termed phototropism, and this phenomenon guides the growth of many photosynthetic species as well as other organisms such as coral.[41-43] The morphological phenotypes displayed by such organisms thus reflect the light available in the habitat during growth.[44,45] Herein, a biomimetic process based on responsive phototropic growth of materials termed "inorganic phototropic growth" is explored. Inorganic phototropic growth enables directed morphology generation via anisotropic material addition towards optical field intensity with mesostructural intricacy resulting as a consequence of the asymmetries of the light-material interactions intrinsic to the process.

1.2 Inorganic Phototropic Growth
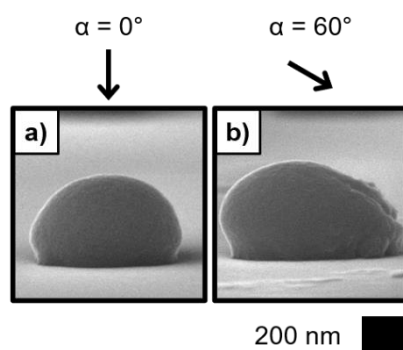
Figure 1.2. Directional inorganic phototropic growth. Cross-sectional SEMs representative of photoelectrodeposits generated with λ_{avg} = 528 nm illumination incident at the indicated angle ⟑ from the substrate normal.

Spatially directed, inorganic phototropic growth of isolated Se-Te deposits can be generated in response to manipulation of the direction of a spatially conformal, incoherent, and unpolarized beam of light.[46] Se-Te has been electrochemically grown via cathodic electrodeposition from an aqueous solution of 0.020 M SeO_2, 0.010 M TeO_2 and 2.00 M H_2SO_4 under illumination on circular Au islands that were lithographically patterned onto an n^+-Si substrate. The feature size and pitch of the Au islands were designed to minimize optical and electrochemical communication between adjacent regions of growth. Such isolation enabled investigation of the intrinsic material growth behavior independent of emergent phenomena, including array effects, which may dominate the growth characteristics of an unconstrained, extended film. Figure 1(a) and (b) present representative cross-sectional scanning-electron micrographs (SEMs) of isolated Se-Te deposits generated using a narrowband light-emitting diode (LED) source with an intensity-weighted average wavelength, λ_{avg}, of 528 nm, with the illumination incident at the indicated angle, α, from the surface normal. With α = 0° (normal incidence, Figure 1.2(a)), a symmetrical, hemispherical cross-

section was observed. For α = 60° (Figure 1.2(b)), the deposit cross-section was somewhat

hemispherical but exhibited marked asymmetry in that greater mass was observed on the side

of the incident illumination relative to the opposite side.
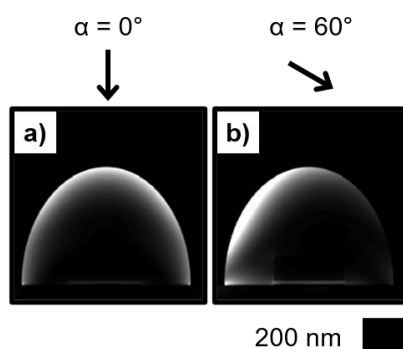
Figure 1.3. Simulated light absorption profiles in a model photoelectrodeposit morphology. Modeled using λ_{avg} = 528 illumination incident at the indicated angle α from the substrate normal.

To provide insight into the relation between the material absorption and the observed

phototropic response, light absorption simulations were performed using full-wave

electromagnetic simulations. Figure 1.3(a) and (b) presents graphical representations of the

light absorption profiles calculated for the model structure using λ_{avg} = 528 nm for α = 0 and

60°. For α = 0° (Figure 3a), the absorption profile was symmetrical and most of the absorption

was strongly localized near the growth (solution) interface. With α = 30° (Figure 3b) the

absorption was also tightly confined near the solution interface but was asymmetrically

distributed spatially, with greater absorption on the side of the incident illumination. The

extent of asymmetry in the absorption profiles correlated with the morphological anisotropies

observed experimentally (Figure 1.2).
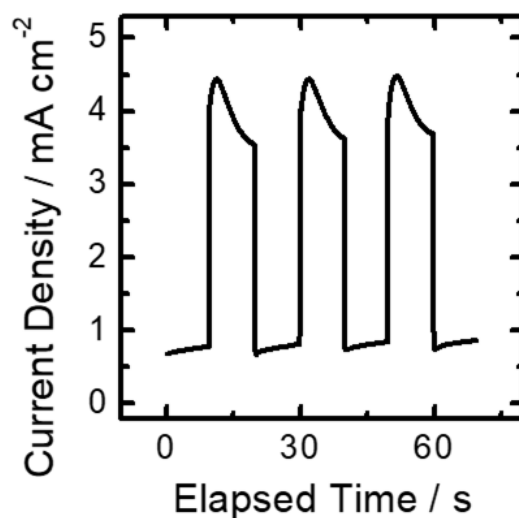
Figure 1.4. Chronoamperometry data for light-mediated cathodic Se-Te electrodeposition. Data acquired using a polarization of E = -0.400 V vs. Ag/AgCl (3M) in a solution of 0.020 M SeO_2, 0.010 M TeO_2, 2.00 M H_2SO_4 with λ_{avg} = 528 nm illumination with a power of P = 14.5 mW cm^{-2} shuttered at 0.1 Hz.

Figure 1.4 presents chronoamperometry data for light-mediated Se-Te electrodeposition with shuttered illumination. The deposition current density is observed to be significantly higher under illumination than in the dark. This data, along with the light absorption simulations (Figure 1.3) indicate that the observed inorganic phototropic growth response (Figure 1.2) arises from spatially anisotropic absorption in the growing deposits, which in turn promotes locally elevated rates of electrochemical growth where absorption is high, resulting in directional growth.
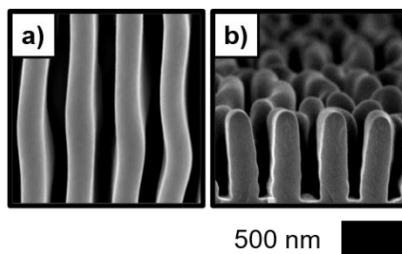
Figure 1.5. Inorganic phototropic growth with an unpatterned substrate and unstructured illumination. (a) Top-down SEM representative of a Se-Te photoelectrodeposit generated with vertically polarized λ_{avg} = 955 nm illumination. (b) Same as (a) but cleaved along the horizontal axis and acquired in cross-section.

Inorganic phototropic growth on unpatterned substrates using incoherent, uncorrelated illumination with spatially-invariant intensity can spontaneously generate films highly ordered, anisotropic mesostructures with nanoscale features over macroscale areas (cm^2).[47,48] Such structures are formed without the use of a photomask or any physical or chemical templating agents.[10,11,49-52] Figure 1.5 presents a representative top-down SEM of a photoelectrodeposit generated via inorganic phototropic growth using vertically polarized λ_{avg} = 955 nm illumination from an incoherent LED source. The SEM reveals a highly anisotropic lamellar morphology wherein the long axes of the lamellae are oriented parallel to the polarization axis. Figure 1.5(b) presents an analogous SEM to that in Figure 1.5(a) that was acquired in cross-sectional view from a sample that had been cleaved along the horizontal axis (perpendicular to the direction of polarization), providing a view down the lamellar axis and highlighting the high aspect ratio of the lamellar features and thus the substantial out-of-plane anisotropy of the photoelectrodeposit. Such template-free mesostructure growth demonstrates the capacity of inorganic phototropic growth to spontaneously generate defined nanoarchitectures.
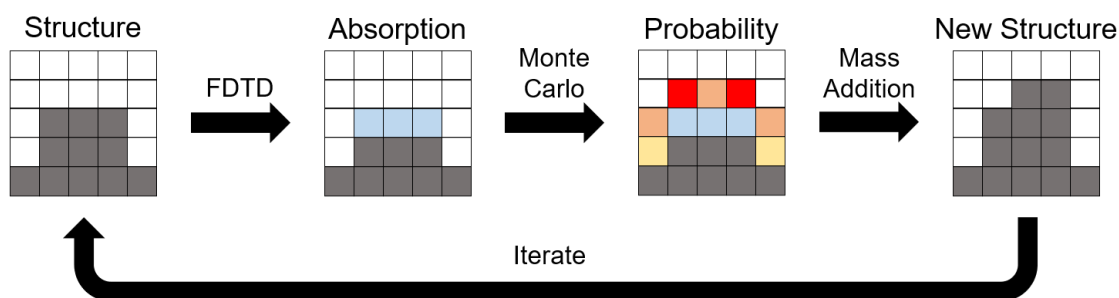
Figure 1.6. Schematic summarizing the optically-based iterative growth model used to computationally assess inorganic phototropic growth. First, full-wave electromagnetic simulations using a finite-difference time-domain (FDTD) technique are performed to calculate the spatially-dependent light absorption profile. This is used to weight the probability of mass addition in a Monte Carlo routine. The process is then iterated to simulate continued growth.

Inorganic phototropism has been explored computationally using an optically-based, two-step iterative growth model that is graphically summarized in Figure 1.6. First, full-wave electromagnetic simulations are performed using a finite-difference time-domain method (FDTD) to determine the spatially dependent profile of light absorption at the growth interface. A Monte Carlo method is then used to add mass with a spatial probability weighted by the absorption calculated in the initial step. Empirical inputs were minimal and included estimates of the deposit complex refractive index and the electrolyte index.
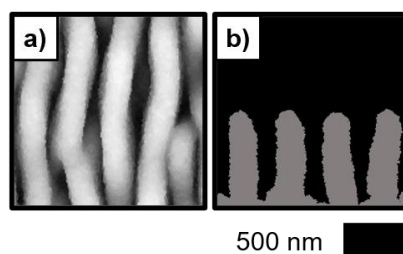
Figure 1.7. Simulated morphologies for inorganic phototropic growth with an unpatterned substrate and unstructured illumination. Se-Te growth modeled using vertically polarized $\lambda_{avg} = 955$ nm illumination in (a) three dimensions and (b) two dimensions.

Figure 1.7 presents simulated morphologies analogous to the experimental data presented in Figure 1.5. Close agreement between the experimental and computational data indicates that the empirical structures are principally determined by optical processes as opposed to any (electro)chemical or crystallographic bias of the Se-Te material during growth.[53-55] Additionally, similar inorganic phototropic growth has been utilized to generate structures of crystalline PbSe and CdSe, and the same optically-based model used to simulate Se-Te growth successfully reproduced the morphologies of these materials with only the same set of limited empirical inputs.[56,57] These data demonstrate the generality of the process and suggest that it may be applied to direct the growth of a wide range of semiconductor materials. With such impetuses we began and now continue to explore the precise manner by which specific optical inputs result in precise mesoscale morphologies.[58-62]

1.3 Overview

The following chapters explore the physical translation of defined optical excitation inputs into mesostructured morphological outcomes via inorganic phototropic growth and the underlying physical mechanisms. Chapter 2 provides the experimental and computational methods utilized in this investigation. Chapter 3 explores the response to the input wavelength and spectral distribution. Chapter 4 investigates control using linearly polarized inputs and Chapter 5 the expression of the relative phase and coherence of such inputs.